# OBSERVING MODE ATTITUDE CONTROLLER FOR THE LUNAR RECONNAISSANCE ORBITER

**Philip C. Calhoun and Joseph C. Garrick**
**NASA Goddard Space Flight Center, Code 595, Greenbelt, MD, 20771**

## ABSTRACT

The Lunar Reconnaissance Orbiter (LRO) mission is the first of a series of lunar robotic spacecraft scheduled for launch in Fall 2008. LRO will spend at least one year in a low altitude polar orbit around the Moon, collecting lunar environment science and mapping data to enable future human exploration. The LRO employs a 3-axis stabilized attitude control system (ACS) whose primary control mode, the "Observing mode", provides Lunar Nadir, off-Nadir, and Inertial fine pointing for the science data collection and instrument calibration. The controller combines the capability of fine pointing with that of on-demand large angle full-sky attitude reorientation into a single ACS mode, providing simplicity of spacecraft operation as well as maximum flexibility for science data collection. A conventional suite of ACS components is employed in this mode to meet the pointing and control objectives.

This paper describes the design and analysis of the primary LRO fine pointing and attitude re-orientation controller function, known as the "Observing mode" of the ACS subsystem. The control design utilizes quaternion feedback, augmented with a unique algorithm that ensures accurate Nadir tracking during large angle yaw maneuvers in the presence of high system momentum and/or maneuver rates. Results of system stability analysis and Monte Carlo simulations demonstrate that the observing mode controller can meet fine pointing and maneuver performance requirements.

## INTRODUCTION

The Lunar Reconnaissance Orbiter (LRO) mission is the first of a series of lunar robotic spacecraft scheduled for launch in Fall 2008. LRO will spend at least one year in a low altitude polar orbit (mean altitude approx. 50km) around the Moon, collecting lunar environment science and mapping data to enable future human exploration. The objective is to provide key science data necessary to facilitate human return to the Moon as well as identification of excellent opportunities for future science missions. LRO's instrument suite will provide the high resolution imaging data with sub-meter accuracy, highly accurate lunar cartographic maps, and mineralogy mapping, amongst other science data of interest.

The LRO employs a 3-axis stabilized attitude control system (ACS) whose primary control mode, the "Observing mode", provides Lunar Nadir, off-Nadir, and Inertial fine pointing for the science data collection and instrument calibration operations. The Observing mode controller is required to maintain fine pointing during the operation of a large fully-articulated solar array that maintains solar incidence normal to the array surface. This mode is also required to maneuver to off-Nadir attitudes, ensuring opportunities for capturing important science data. In addition, large angle maneuvers are required for the purposes of performing delta-V and station keeping operations, solar array pointing, instrument calibration, and Nadir attitude acquisition from Sun pointing or other inertial attitudes. A conventional suite of ACS components is employed in this mode to meet the pointing and control objectives. Actuation is provided by a set of four reaction wheels developed in-house at NASA Goddard Space Flight Center (GSFC), with momentum unloading provided by a reaction control system (RCS) also developed in-house. The attitude determination function utilizes two Galileo Avionica Autonomous Star Trackers (A-STR), and a single Honeywell Miniature Inertial Measurement Unit (MIMU).

The Observing mode controller is required to provide fine Nadir pointing with an absolute accuracy of 45 arc-sec (3 sigma) and knowledge of 30 arc-sec (3 sigma) measured relative to the prime AST reference. An on-board ephemeris interpolator generates Nadir attitude targets used for nominal science data collection. Attitude determination is performed by a six-state Multiplicative Extended Kalman Filter (MEKF) with three attitude states

and three IRU drift bias states.[1, 2] This filter has flown on previous missions, most recently the Wilkinson Microwave Anisotropy Probe (WMAP), and is also planned to provide onboard attitude for the Solar Dynamics Observatory (SDO) mission. The Observing mode combines the capability of fine pointing with that of on-demand large angle full-sky attitude reorientation to provide simplicity of spacecraft operation as well as maximum flexibility for meeting science data collection objectives.

This paper describes the design and analysis of the Observing mode controller. The first section describes the suite of ACS components used in the controller. Next, a detailed description of the controller design is given. This controller utilizes quaternion feedback, augmented with a unique algorithm that ensures accurate Nadir tracking during large angle yaw maneuvers. Results of Monte Carlo simulations of fine pointing and large-angle attitude maneuver scenarios are used to demonstrate controller performance.

## ACS HARDWARE

A conventional suite of ACS components is employed in the Observing mode to meet the pointing objectives for LRO. Actuation is provided by a set of four reaction wheels, developed in-house at the Goddard Space Flight Center. Wheel momentum unloading is provided by a reaction control system (RCS) comprised of eight thrusters arranged in two banks. Wheel momentum unloading is performed in a separate control mode (Delta-H) and will not be addressed in this paper. Attitude determination is performed utilizing two Galileo Avionica Autonomous Star Trackers (A-STR), and a single Miniature Inertial Measurement Unit (MIMU) manufactured by Honeywell.

### Miniature Inertial Measurement Unit (MIMU)

The LRO Honeywell MIMU unit does not include a 3-axis accelerometer and thus is configured as an Inertial Reference Unit (IRU). Table 1 gives the performance parameters of the IRU relevant to this study. The IRU is a three-axis unit and is nominally aligned with the spacecraft's body axis. It employs three ring laser gyros mounted in a single unit with the input axes mutually orthogonal to each other. The IRU has low noise and drift for providing accurate rate measurement for fine attitude navigation when used with Star Tracker quaternion data in an onboard Kalman filter. The IRU rate is used to propagate the onboard attitude estimate without star tracker measurement updates when the Kalman filter attitude estimate is not selected for use, or star tracker quaternion data is not valid.

Table 1. IRU Performance Parameters

| Parameter | Requirement |
|---|---|
| Angle Random Walk ($\sigma_U$) | 7.0 e-5 arc-sec/sec$^{3/2}$ |
| Rate Random Walk ($\sigma_V$) | 0.3 arc-sec/sec$^{1/2}$ |
| Readout Noise ($\sigma_E$) | 1.0 arc-sec |
| Scale Factor stability (after calibration) | 100 ppm ($3\sigma$) |

### Autonomous Star Tracker (A-STR)

To meet the fine pointing requirements of the mission, two Galileo Avionica Autonomous Star Trackers (A-STR) are utilized for attitude determination during Observing mode control. The LRO required accuracies for each star tracker are given in Table 2. The A-STR tracker is a quaternion tracker that outputs its quaternion relative to the J2000 Earth Centered Inertial (ECI) reference frame. The attitude knowledge of the system is primarily affected by the level of the bias and systematic errors. Therefore, two A-STR are needed to achieve the required attitude knowledge performance. The boresights of the two star trackers are aligned sixty degrees apart, providing at least one functional A-STR during occasional star tracker occultation from Earth or Sun within the A-STR field of regard. Star tracker quaternion data is validated, for use in the Kalman filter, by post-processing the A-STR measurement onboard. A-STR quaternion validation includes checks on the quaternion norm, change in quaternion output, predicted A-STR occultation from Earth, Moon, or Sun within the A-STR field of regard, and A-STR data quality index.

Table 2. Star Tracker Performance Parameters

| Parameter | Requirement (Attitude rate < 0.3 deg/sec) | |
|---|---|---|
| (All errors are shown for output quaternion) | | |
| | Bias + Systematic (arc-sec, 3 σ) | Random (arc-sec, 3 σ) |
| Transverse Error | 11 | 36 |
| Roll about Boresight Error | 30 | 120 |

**Reaction Wheels**

The LRO spacecraft has four reaction wheels onboard to provide control torque during the Observing control modes. The wheels are sized to provide adequate momentum storage to meet the momentum dumping frequency requirement of two weeks. The reaction wheels are manufactured at NASA/GSFC by the Component Hardware Systems Branch, in the Mission Engineering and Systems Analysis (MESA) Division. The four wheels are aligned in pyramid fashion with the apex of the pyramid centered on the spacecraft's +X body axis. This alignment was determined as the best for the expected momentum accumulation. A level of redundancy exists in case of a single wheel failure. However, in this condition the ACS can not meet the two week momentum unloading interval. Table 3 provides a list of the reaction wheel performance requirements relevant to this study. The momentum capacity of 80 N-m-sec is the requirement for low bus voltage of 24 Volts. The 60 N-m-sec level is the maximum level expected before momentum unloading during typical science operations. The torque noise requirement is a PSD specification on the allowable broadband noise below 1 Hz. Reaction wheel imbalance requirements are not given in this paper since their jitter effects, along with all other jitter sources, are not considered part of the ACS pointing accuracy budget.

Table 3. Reaction Wheel Performance

| Parameter | Requirement |
|---|---|
| Momentum Capacity | 80 N-m-sec<br>60 N-m-sec (nominal limit) |
| Maximum Torque Cmd | 0.16 N-m |
| Torque Noise (root PSD) | 3e-4 N-m/Hz$^{1/2}$ |
| Coulomb Friction | +/- 0.004 N-m |
| Torque Cmd. Quantization | 15 bit (D/A) |

**OBSERVING CONTROLLER**

The Observing controller is a quaternion-feedback, proportional-integral-derivative (PID) controller used to produce reaction wheel torque commands. A mathematical description of the body control torque, $\vec{T}_c$, is provided by Equation 1. In this equation, the first three terms are referred to as the PID torque, denoted as $\vec{T}_{PID}$, and the last term is referred to as the gyroscopic compensation term. This form of the controller is similar to the quaternion feedback control law presented in Ref. 3. The body control torque is comprised PID terms involving rate error, $\bar{\omega}_e$, attitude error, $\vec{a}_e$, and integral of attitude error, using the feedback gains $k_r, k_p,$ and $k_i$. The following parameters are also included in the definition of the body control torque; $I_B^{B^*}$, the Inertia matrix of the spacecraft about its mass center $B^*$, $\vec{h}_W$, RW angular momentum, and, $\bar{\omega}_B$, the estimated spacecraft body rate.

$$\vec{T}_c = I_B^{B^*}\left(k_r\bar{\omega}_e + k_p \text{proplim}[\bar{a}_e] + k_i\int \bar{a}_e\right) + \bar{\omega}_B \times (I_B^{B^*}\bar{\omega}_B + \vec{h}_W) \qquad (1)$$

The PID gains, given in Table 4, are set to yield a -3dB bandwidth of 0.1 Hz, approximately equal to one tenth of the lowest frequency flexible mode of the spacecraft. An anti-windup integration scheme is used to limit the integral term. During large angle slews the integral term is set to zero to avoid overshoot or instability from integral feedback. The gyroscopic compensation term is included in the controller to compensate for gyroscopic cross-coupling due to high system momentum conditions, providing a form of feedback linearization for the controller.

The attitude error vector is given in Equation 2. The overbar notation represents the vector part of the error quaternion, where $q_{Est}$ is the estimated attitude quaternion and $q_{Tar}$ is the target attitude quaternion.

$$\bar{a}_e = 2 * \overline{[q_{Est}^{-1} \otimes q_{Tar}]} \tag{2}$$

Equation 1 differs slightly from the quaternion feedback control law [3], which implements large-angle, slew rate constrained, inertial eigen-axis maneuvers. Differences include the feedback of a specially computed rate error, $\bar{\omega}_e$, and the use of proportional limiting on quaternion error for preservation of the attitude vector direction. These two differences were implemented to maintain accurate Nadir pointing during large angle slews relative to the instantaneous Nadir reference frame. LRO performs these 180 deg yaw maneuvers relative to the Nadir frame every four weeks to set up the spacecraft attitude for delta-V station keeping maneuvers. Two delta-V burns are performed in opposite directions along the velocity vector at one-half orbit intervals to maintain the relatively unstable, low-altitude lunar orbit. Reorientation of the solar array, depending upon the solar beta angle, requires two additional yaw maneuvers performed twice per year. During these yaw slews LRO should maintain Nadir target tracking, primarily to avoid Sun exposure within each science instrument field of view (FOV).

The rate error feedback term, given in Eq. 3, is the difference of the estimated spacecraft body rate, $\bar{\omega}_B$ and the Nadir base target frame rate resolved in instantaneous body coordinates, $\bar{\omega}_{Tar}{}^B$. For inertial targets, the base frame rate is zero and this error term simplifies to the rate feedback for the controller in Ref. 3.

$$\bar{\omega}_e = \bar{\omega}_{Tar}{}^B - \bar{\omega}_B \tag{3}$$

The Nadir base rate provides a feedback term that tends to establish the coordinated roll/pitch motion necessary to maintain tracking of the instantaneous base Nadir frame. Since the attitude error is limited and the attitude feedback gain is relatively small, the rate feedback term tends to dominate the PID control torque. Yaw motion control is ensured by proportionally limiting the quaternion feedback to maintain a body yaw torque in the direction of the commanded maneuver. Since the yaw control dynamics are essentially decoupled from the roll/pitch rate control dynamics, due to the feed forward of the gyroscopic coupling terms, each control motion task can be accomplished without significantly disturbing the other. The kinematic coupling of rate error and angle error feedback is avoided by this axes decoupling. The resulting motion approximates a pure yaw slew about the local Nadir, maintaining Nadir targeting during the large angle maneuver.

A third-order elliptic filter, applied to each body axis torque, is used to provide modal suppression of the low frequency spacecraft modes while maintaining adequate linear stability margins. The structural filter parameters are given in Table 4.

The commanded wheel torques, $\vec{T}_W$, are expressed as a sum of the filtered command torques, $\vec{T}_{c\,filt}$, expressed in the wheel space by the reaction wheel alignment matrix, $A_{WB}$, wheel drag compensation torque, $\vec{T}_{Wdrag}$, and wheel momentum redistribution torque, $\vec{T}_{h_W redist}$. Proportional limiting is applied to the wheel torque commands in the baseline controller algorithm to provide an acceptable command range for the commanded wheel torques.

$$\vec{T}_W = \text{proplim}[-A_{WB}\vec{T}_{c\,filt} + \vec{T}_{Wdrag} + \vec{T}_{h_W redist}] \tag{4}$$

An alternative approach, that preserves the PID control torque vector direction when the RW commands are saturated, is described in the next section.

The wheel momentum redistribution torque is computed using the Mini-Max wheel momentum redistribution law [4], given in Eq. 5, where $k_{h_W redist}$ is the wheel momentum redistribution gain given in Table 4. This law tends to minimize the maximum of the individual wheel momentum, thus tending to drive pairs of wheels at the same speed in the same direction. The limit in Eq. 5 is set to 0.02 N-m in the simulation studies performed for LRO.

$$\vec{T}_{h_W redist} = \lim\left[ -k_{h_W redist} \tfrac{1}{2}\left(\max(h_W) + \min(h_W)\right)\right] \tag{5}$$

Table 4. Observing Controller Parameters

| Parameter | Symbol | Value |
|---|---|---|
| Rate gain | $k_r$ | 0.4 $sec^{-1}$ |
| Position gain | $k_p$ | 0.057 $sec^{-2}$ |
| Integral gain | $k_i$ | 0.0023 $sec^{-3}$ |
| Wheel Mom. Redist. gain | $k_{h_W redist}$ | 0.01 N-m |
| Structural filter ($3^{rd}$ order) | | Passband ripple = 0.1 dB<br>Stopband Attenuation = 35 dB<br>Roll-off frequency = 0.35 Hz |

**Alternate RW Torque Command**

The LRO baseline algorithm for determining the wheel torque commands is given by Eq. 4. The proportional limiting is performed on the sum of the filtered control torque, drag compensation, and momentum redistribution torques. This method has a potential defect; it does not necessarily preserve the direction of the filtered PID torque when RW commands exceed the proportional limits. An alternative method for implementing the wheel torque commands is motivated from the fact that it is important to preserve the filtered PID torque direction to produce the desired motion control during large angle slews, as discussed in the previous controller section. This is accomplished by applying proportional limiting separately to the filtered PID torques. It is also important to preserve the other torques, particularly the gyroscopic compensation torques, which dominate the RW commands when the system momentum is high. Of course there is a trade-off between limiting the RW compensation torques versus the filtered PID torques when torque saturations occur.

The solution is to first map the gyroscopic compensation torques to wheel space, and then compute a limited RW compensation torque expressed in wheel space, $\vec{T}_{RWcomp\lim}{}^{W}$, as shown in Eq. 6. This limit ensures that there will be some residual wheel torque available for the filtered PID control torque, so that the system can be stabilized and the maneuver completed successfully. In practice this residual torque can be quite small for the controller to still maintain the slew performance.

$$\vec{T}_{RWcomp\lim}{}^{W} = \lim\left[ A_{WB}\left[\vec{\omega}_B \times (I_B^{B^*}\vec{\omega}_B + \vec{h}_W)\right] + \vec{T}_{Wdrag} + \vec{T}_{h_W redist}\right] \tag{6}$$

Now, compute the upper bound on the filtered PID torque allowed for each wheel, $T_{PID\,filt}{}^{W}\big|_{Ubnd}$. This is accomplished by subtracting the limited RW compensation torques from the total upper bound on the wheel commands, $\vec{T}_W\big|_{Ubnd}$. The numerical values computed for each wheel's upper bound are dependent upon the signs of the filtered PID torques expressed in wheel space, $\vec{T}_{PID\,filt}{}^{W}$, as shown in Eq. 8. This produces a larger value for the allowable filtered PID torques when the RW compensation torques are in opposite directions.

$$\vec{T}_{PID\,filt}{}^{W} = -A_{WB}\,\vec{T}_{PID\,filt} \tag{7}$$

$$\vec{T}_{PID\,filt}{}^{W}\Big|_{Ubnd} = \vec{T}_{W}\Big|_{Ubnd} - sign(\vec{T}_{PID\,filt}{}^{W}) \cdot \vec{T}_{RWcomp\lim}{}^{W} \tag{8}$$

Proportional limiting is then applied to the filtered PID control torques by considering the allowable filtered PID torque for each wheel using the algorithm given in Eq. 9 and 10, where $k_{prop\lim}$ is the scale factor for the proportional limiting.

$$k_{prop\lim} = \max\left\{ abs\left( \left. \frac{\left[\vec{T}_{PID\,filt}{}^{W}\right]_i}{\left[\vec{T}_{PID\,filt}{}^{W}\Big|_{Ubnd}\right]_i} \right|_{i=1:4} \right) \right\} \tag{9}$$

$$\vec{T}_{PID\,filt\lim}{}^{W} = \begin{cases} \vec{T}_{PID\,filt}{}^{W} \Big/ k_{prop\lim} & \text{if} \quad k_{prop\lim} > 1 \\ \vec{T}_{PID\,filt}{}^{W} & \text{if} \quad k_{prop\lim} \le 1 \end{cases} \tag{10}$$

Then the wheel torque command is the sum of the limited filtered PID control torque and the RW compensation torques expressed in wheel space.

$$\vec{T}_{W} = \vec{T}_{PID\,filt\lim}{}^{W} + \vec{T}_{RWcomp\lim}{}^{W} \tag{11}$$

This alternative method for computing the RW torque command was compared with the baseline approach using results from the LRO high fidelity simulation. Results of these simulations revealed no significant performance improvement for large angle slew performance for yaw slew rates of 0.1 deg/sec, using the LRO model parameters. Furthermore, difficulties arose during flight software implementation due to the compartmentalization of the ACS body torque command processing from the RW actuator torque command processing, which is computed in a separate software task. For these reasons the baseline design algorithm for computing the RW torque commands, given in Eq. 4, was selected for implementation in the onboard ACS software.

**Stability Analysis**

A linear system stability analysis is performed for the Observing controller to assess the stability of the closed loop system during nominal science data collection operations. During these operations the attitude errors and RW torque commands are not expected to reach their limits. Therefore, linear analysis is sufficient to establish system stability. Control gains and structural filters were tuned to meet NASA Goddard stability margins and modal suppression requirements. The stability and modal suppression requirements for LRO are: gain margin greater than 6 dB, phase margin greater than 30 deg, and modal suppression greater than 12 dB. The system model used for linear stability analysis includes rigid body dynamics, PID controller, structural filter, low frequency flexible modes (less than 20 Hz), and fundamental slosh modes (approx. 1Hz). The following lags were also included in the model; RW dynamics (6 Hz), IRU response (7 Hz), and a one cycle delay (0.2 sec). The controller gains and structural filter parameters used in the analysis are given in Table 4.

The spacecraft flexible modes, used for the stability analysis, were determined from finite element modeling (FEM) of six spacecraft configurations involving selected solar array (SA) and high gain antenna (HGA) gimbal orientations. Since FEM modeling was not available for all possible SA and HGA orientations, a comprehensive survey of the low frequency modes for the entire range SA and HGA gimbal orientations was conducted using a linearized model from a multi-body dynamics analysis. This analysis revealed that the selected configurations for FEM analysis bounded the worst case modal gains for the low frequency spacecraft modes. The flexible modes are

all modeled with 0.1 % damping with the exception of the slosh mode which is modeled with 1% damping. Slosh mode damping is set to one tenth of the expected value to ensure conservative results since this mode tends to interact with the SA modes and reduce damping for the low frequency system modes.

The stability analysis is conducted by breaking the control loop at three locations; angle, rate, and torque feedback. Margins were evaluated for nominal model parameters with selected parameter variations. These included +/- 20% variations for Inertias, flexible mode gains, slosh mass, and slosh stiffness, and +/- 25% variations for flexible mode frequencies. Worst case margins over all FEM configurations for the nominal control parameters with parameter variations are shown in Table 5. Breaking the loop at the torque feedback results in the lowest predictions for gain margin (9.5 dB) and modal suppression (12.9 dB); while breaking at angle feedback results in the lowest phase margins (39.2 deg). The lowest frequency structural modes had frequencies of approximately 1 Hz.

Results of the stability analysis demonstrated that all structural modes are gain stabilized with adequate stability margins. Some of the low frequency modes have large modal gain, which, when coupled with the rather conservative assumption of 0.1 % modal damping, made the modal suppression requirement difficult to achieve. A 3rd order elliptic filter is used for structural mode filtering in order to meet the modal suppression requirement in the presence of parameter variations.

Table 5. Summary of Linear Stability Analysis Results (lowest margins obtained are highlighted)

| | **Break at Torque** | | | **Break at Angle** | | | **Break at Rate** | | |
|---|---|---|---|---|---|---|---|---|---|
| **Flex Body (Param. Variations)** | **X axis** | **Y axis** | **Z axis** | **X axis** | **Y axis** | **Z axis** | **X axis** | **Y axis** | **Z axis** |
| Gain Margin (dB) | 9.5 | 9.5 | 9.9 | 16.0 | 16.0 | 16.0 | 11.8 | 9.9 | 9.9 |
| Phase Margin (deg) | 46.7 | 44.6 | 44.2 | 45.2 | 39.2 | 39.2 | 59.1 | 51.3 | 51.1 |
| Modal Suppression (dB) | 12.9 | 13.7 | 14.6 | 47.2 | 47.4 | 50.2 | 30.3 | 13.9 | 14.8 |

**SIMULATION STUDIES**

The observing mode controller is analyzed in several simulation studies using a high fidelity Monte Carlo simulation of the closed loop dynamics to demonstrate worst case expected ACS performance. The spacecraft ephemeris is simulated for a circular orbit with nominal altitude of 50 km above the Lunar surface. The simulation includes rigid body system dynamics with time varying system inertia due to SA and HGA gimbal motion. Nominally, when the Observing controller is operational, the SA is gimbaled to track the Sun and the HGA is gimbaled to track Earth ground stations. The simulation also includes high fidelity models of the ACS flight hardware, data interfaces, and ACS algorithms, as well as environmental disturbances due to gravity gradient and solar pressure. This model, developed using Matlab's Simulink toolbox, is used by the LRO ACS analysis team to assess ACS performance and validate the ACS flight algorithms. Monte Carlo variables include all sensor and actuator error sources, initial body rates, initial RW momentum, and inertias. For each scenario described below the initial RW momentum is varied within the expected range (60 N-m-sec) during Observing mode operations, and the spacecraft inertia is varied by +/- 20% from the nominal values.

The simulation includes error source and disturbance models for the A-STR, IRU, and RW each at their respective requirement levels for assessment of the worst case pointing performance. The AST model includes random noise and bias/systematic errors at the required LRO performance specifications, given in Table 2. AST performance degradation due to ST occultation from the Sun, Earth, and Moon entering within the A-STR FOV is also modeled in the simulation. The IRU noise parameters, including scale factor variations, are modeled at the LRO requirements levels given in Table 1. In addition, slowly varying misalignments due to thermal effects between the IRU and A-STR mounting were modeled with a magnitude of 100 arc-sec ($3\sigma$). Disturbance source models for the RW include wheel friction, torque noise, and torque command quantization at the LRO requirements levels given in Table 3. A nominal RW drag model is also included in the model.

Results of two simulation scenarios are shown in this section to demonstrate the Observing mode performance in two critical operational modes. A Nadir pointing scenario is shown to demonstrate the controller performance

during typical science data collection operations in low lunar orbit. A yaw slew scenario is shown to demonstrate the slew capability of the Observing controller during occasional large angle attitude maneuvers, performed to set up for delta-V operations.

**Nadir Pointing Scenario**

The Observing mode controller is analyzed in a Nadir pointing scenario using the high fidelity simulation to demonstrate worst case expected pointing performance during typical science data collection operations. Each simulation case lasted for one orbit. The time of year is varied randomly to analyze different beta angle conditions, as well as positive and negative velocity vector forward Nadir attitudes. The simulation is initialized with the appropriate Nadir attitude, depending upon time of year, and a nominal body pitch rate of 0.05 deg/sec. ACS hardware error and disturbance sources were modeled at their requirement levels, therefore results shown below illustrate worst case expected performance. Attitude error results from 50 Monte Carlo cases, shown in Figures 1 and 2, demonstrate that the Observing mode controller design can meet the 45 arc-sec (3 sigma) pointing accuracy performance requirement in the presence of marginal ACS hardware performance. Reduced levels of actual ACS hardware performance parameters will result in improved pointing performance during the mission. The attitude errors were dominated by the attitude determination error, primarily a function of the Kalman filter error, and the ST bias / systematic errors. Coulomb friction and tachometer errors at zero speed crossings did not result in significant attitude transients, and thus did not substantially affect the attitude statistics shown in Figure 1. The outliers in the attitude statistics result primarily from attitude estimation errors induced by A-STR occultation when the Earth is within the FOV of one of the A-STR. For all cases, the torques required to maintain Nadir targeting are below 0.05 Nm, and the individual RW momenta remain within the expected RW operating range.

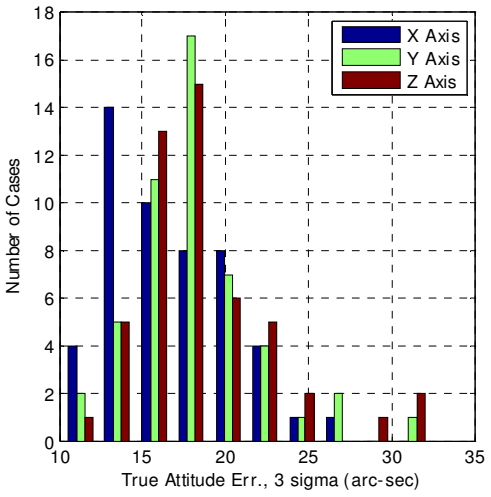


Figure 1, Nadir Scenario, Attitude Error

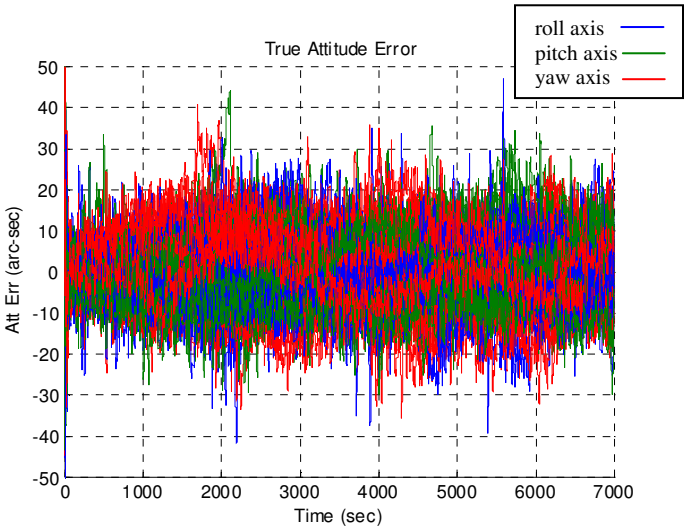


Figure 2, Nadir Scenario, Body Rates

**Yaw Slew Scenario**

The Observing mode controller is analyzed in a typical large angle slew scenario, exercised at four week intervals, to set up the spacecraft attitude for station keeping burns performed for orbit maintenance[5]. This operation involves a sequence of two burns performed in opposite velocity vector directions at intervals of one-half orbit period (approx. 56 min.). This yaw maneuver scenario begins after completion of the first station keeping burn performed in a positive X velocity vector attitude when the ACS mode is transitioned from Delta-V to Observing mode control. Random initial attitude rates of 0.5 deg/sec ($3\sigma$) for each axis were used to approximate the expected worst case rates upon ACS mode transition. The required 180 deg yaw maneuver is initiated 10 min after mode transition to allow sufficient time for the Observing controller to damp attitude rates and stabilize the attitude. No momentum unloading is assumed, so the initial wheel momenta were set within the expected range during typical Nadir operations. The attitude error limit is set to maintain the required slew rate of 0.1 deg/sec. The yaw slew is completed approximately 40 minutes after mode transition, allowing approximately 16 min. to transition back to

Delta-V mode to begin the second burn. If more time is required to set up for the second burn the slew rate could be set higher by setting the appropriate attitude error limit. But, within the operating range of wheel momentum the wheel torques would likely exceed their limits as the slew rate increases above 0.1 deg/sec. In this situation wheel momentum unloading would be need to be performed prior to the first burn.

Results for 50 Monte Carlo simulation cases of this scenario are shown below in Figures 3 and 4. Initial rate damping and attitude stabilization is completed within 5 min after mode transition in all cases. The yaw maneuver is initiated at 10 min after controller mode transition and is completed in approximately 30 min in all cases. A steady yaw slew rate (0.1 deg/sec), set by the attitude error limit is achieved in all cases. As shown in Figures 3 and 4, the yaw slew is properly coordinated relative to the instantaneous Nadir frame. This results in a pure yaw motion with variable pitch / roll rate as the spacecraft maneuvers from +X velocity vector to the -X velocity vector Nadir attitudes. The off-Nadir roll and pitch attitude excursions are maintained at less than 1 deg during the slew as shown in Figure 3. Relatively large torques, present during the slew, primarily due to counteracting the gyroscopic effects of the RW momentum, nearly reached their limits. This indicates that the RW momentum should be dumped prior to the slew to avoid the potential for RW momentum saturation.

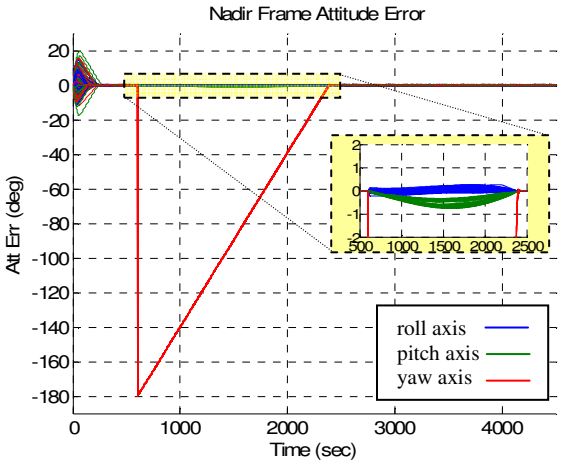


Figure 3, Yaw Slew Scenario, Attitude Error

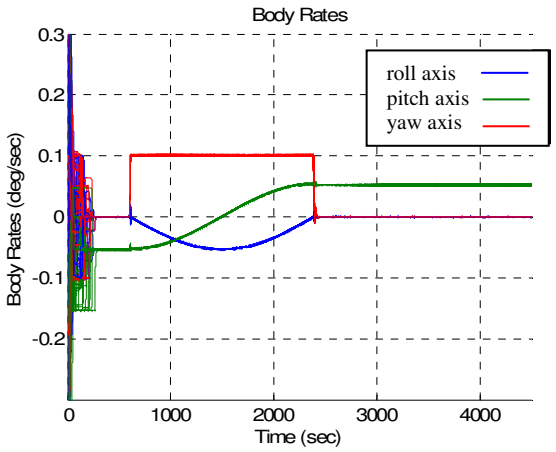


Figure 4, Yaw Slew Scenario, Body Rates

**CONCLUSIONS**

This paper documents the design of the LRO Observing mode controller, which combines fine pointing capability for science data collection operations with full-sky large-angle slew capability into a single ACS control mode. The results from linear system stability analysis and two simulation studies, using the LRO high fidelity simulation, demonstrate the LRO fine pointing and large angle slew performance. The results show robust performance in the presence of parameter variations and marginal ACS hardware performance. Fine pointing and stability requirements are achieved with margin. Nadir target attitude excursions during large angle yaw slews are limited to less than 1 deg, ensuring direct sunlight avoidance for the Nadir pointing instrument suite during occasional 180 deg yaw slews.

An alternate method is developed for computing the RW torque commands, which uses proportional limiting of the filtered PID torque commands to preserve the PID torque vector direction. This method was compared against the baseline approach using the LRO high fidelity simulation. No significant performance improvement has been observed in studies performed to date. For this reason, and because of flight software implementation issues associated with the alternate method, the baseline approach was chosen as the method to carry forward to software development. However, it is thought that the alternative method holds promise to provide improved performance, possibly in scenarios not studied thus far. Future work should perform more extensive studies to determine whether or not this method is useful in improving control performance and stability during large angle slews that induce RW torque saturation.

**REFERENCES**


1) Marley, F.L., "Attitude Error Representations for Kalman Filtering", *AIAA Journal of Guidance, Control, and Dynamics*, Vol. 26, No. 2, March-April 2003, pg 311- 317.

2) Lefferts, E.J., Markley, F.L., and Shuster, M.D., "Kalman Filtering for Spacecraft Attitude Estimation," *Journal of Guidance, Control, and Dynamics*, Vol. 5, No. 5, 1982, pp. 417–429.

3) Wie, B., "Space Vehicle Dynamics and Control", AIAA Education Series, AIAA, Reston, VA., 1998.

4) Mason, P.A.C., Starin, S.R., "SDO Delta H Mode Design and Analysis", *20th International Symposium on Space Flight Dynamics*, Annapolis, Md., September 24-28, 2007,

5) Beckman, M.R., Lamb, R.C., "Stationkeeping for the Lunar Reconnaissance Orbiter (LRO)", *20th International Symposium on Space Flight Dynamics*, Annapolis, Md., September 24-28, 2007,